Artificial Neural Network-based Pole-tracking Method for Online Stabilization Control of Grid-tied VSC

Zhang, Chen; Mijatovic, Nenad; Cai, Xu; Dragicevic, Tomislav

Published in:
IEEE Transactions on Industrial Electronics

Link to article, DOI:
10.1109/TIE.2021.3134079

Publication date:
2022

Document Version
Peer reviewed version

Artificial Neural Network-based Pole-tracking Method for Online Stabilization Control of Grid-tied VSC

Chen Zhang, Nenad Mijatovic, Xu Cai, Tomislav Dragičević

***Abstract*—To cope with the weak grid stability issue of grid-tied Voltage Source Converters (VSCs), this letter proposes an Artificial Neural Network (ANN)-based approach for online stabilization control of the grid-tied VSC with the *pole-tracking* feature. First, an ANN is adopted to establish the mapping between the control parameters and the closed-loop poles of the grid-VSC system, serving as a computationally light model surrogate that is favorable for real-time control applications. Then, an online parameter search algorithm enabling simultaneous tuning of multiple controllers and parameters is developed, by which the system's poles under a new grid condition can be pulled to the reference ones, i.e., achieving the pole-tracking-based stabilization control of this work. Finally, the efficacy of the proposed method along with its stabilization effect is verified by MATLAB simulations and experimental results.**

***Index Terms*—Artificial neural network, impedance, pole-tracking, stability, stabilization control, VSC.**

I. Introduction

VOTLAGE SOURCE CONVERTERS (VSCs) have been widely deployed as the grid interfaces for a variety of renewable sources such as wind and solar. Since the majority of existing grid-interfacing VSCs are current-programmed, they behave like current sources in the power system, tending to decrease the grid strength as the penetration level increases [1] (herein the grid-strength is usually characterized as the Short Circuit Ratio (SCR) and its several variants [1], [2]). Recently, field experiences in operating large-scale VSCs-based resources (e.g., the wind farm case [3] and the solar power plant case [4]) have demonstrated that VSCs are susceptible to stability issues when connected to weak grids. Driven by the emerging stability issues, a large number of studies have been conducted, where the impedance-based approach [5] that was initially put forward in 1976 for input filter design of switching converters [6] is among the most popular adoption. With this method, the stability issue of the grid-tied VSC can be equally studied by the stability of a closed-loop feedback control system; as a result, the well-known Nyquist criterion [7] can be applied for stability analysis and the impedance ratio of the grid and the VSC constitutes the required minor loop gain. Moreover, with this control system representation, instability of the VSC can also be interpreted as the lack of control robustness to the variation of grid impedance.

Regarding the improvement of control robustness, two roadmaps are usually considered: one is to design nonlinear controllers (e.g., the sliding mode control (SMC) [9]) having inherent robustness to the parameter variation of control plant; for the case of grid-tied VSC system, the variation of control plant mainly refers to the variation of grid impedance. Another way of improving control robustness is to adaptively adjust the controller's parameters following the changing grid impedance, where the variation of grid impedance (e.g., *RL*-based) can be estimated online by various time/frequency-domain approaches, e.g., using the extended Kalman filter [10], the Recursive Least Square (RLS) [11][12], and the broadband signal injection-based methods [13]. Adaptive controls achieved by such online parameter tuning approaches can be historically referred to as the auto-tuning technique [14]. Since this technique is more accessible to practitioners compared with the nonlinear controller design, it has long been favorited by industrial applications. Applications of the auto-tuning technique for improving the harmonic distortion of a power factor correction (PFC) rectifier, enlarging the stability region of a grid-tied VSC, and ensuring the maximum allowable control bandwidth tracking of dc Microgrids power converters are, for instance, presented in [15], [16], and [17] respectively. Although these methods are demonstrated to be effective in presented scenarios, the amount of tuned parameters is mostly limited to two/three parameters of a *single* controller (e.g., a PID controller). This implies that when tuning a multi-input and multi-output (MIMO) system, the effects of tuning one channel's control parameters on the other may not be sufficiently accounted for; this is the case of the VSC—a MIMO system with evident couplings between inputs and outputs [18]. Therefore, techniques appropriate for simultaneous tuning of multiple controllers and parameters are expected to be put forward.

Manuscript received Month xx, 2xxx; revised Month xx, xxxx; accepted Month x, xxxx. This work is financially supported by the National Natural Science Foundation of China (Grant No. 51837007).

Chen Zhang and Xu Cai are with the Key Laboratory of Control of Power Transmission and Conversion, Ministry of Education, Shanghai Jiao Tong University (SJTU), Shanghai, 200240, China, and also with the Department of Electrical Engineering, SJTU, Shanghai, 200240, China (email: {nealbc, xucai}@sjtu.edu.cn).

Nenad Mijatovic, and Tomislav Dragicevic are with the Department of Electrical Engineering, Technical University of Denmark (DTU), Lyngby, 2800, Denmark (e-mail:{nm, tomdr} @elektro.dtu.dk).

However, this is not trivial work as the system's complexity will drastically increase when more parameters and controllers are involved, posing great challenges on the tuning law design and the real-time applications. To alleviate this issue, artificial intelligence (AI) techniques can be useful.

AI is a useful tool in handling complex modeling and control issues, as well as being friendly for real-time applications to some extent. An early work [19] applies the Artificial Neural Network (ANN) to serve as an intelligent action network for a grid-tied VSC, showing improved transient response performance. Recently, [20] applies the ANN to find the impedance mapping of the VSC under various operating conditions; [21] trains the ANN as a surrogate of model-predictive-control (MPC) saving much online computational effort; while [22] applies the Deep Reinforcement Learning (DPL) to improve the stability of the dc-dc converter operated with constant power load (CPL), etc. In light of these promising applications of AI in power electronics systems [23], this letter applies the ANN to provide a new perspective for formulating the stability-oriented online parameter-tuning method for VSCs. The developed method not only enables an efficient tuning of multi controller's parameters online but also endows the VSC with a novel *pole-tracking* feature by which stability of the grid-tied VSC under changing grid conditions can be ensured.

II. Methodology

A. Overview of the method

Fig. 1 shows the grid-VSC system used in this work to demonstrate the efficacy of the proposed method. A variable grid inductance (e.g., L_g) is considered to emulate the change of grid strength (i.e., SCR), where the SCR can also be written as: $k_{SCR}=1/\bar{L}_g$ [1] ($\bar{L}_g$ is the per-unit value of the grid inductance L_g). Since k_{SCR} can be estimated various techniques as early mentioned, its value is assumed known in this work.

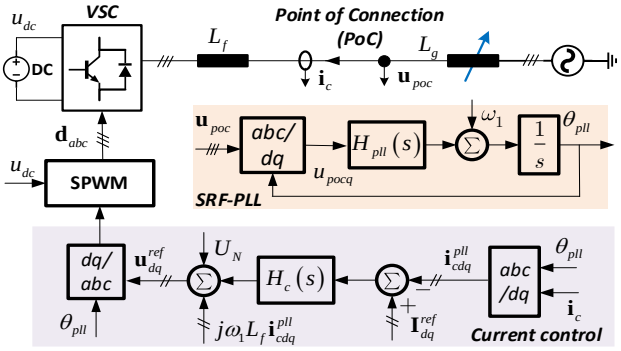

Fig. 1 Schematic of a typical grid-VSC system. A synchronous reference frame (SRF) phase-locked-loop (PLL) is used for grid-synchronization, and dq-frame current vector control is employed for controlling the ac currents of the VSC. Besides, H_{pll} and H_c are typically PI regulators.

Fig. 2 (a) illustrates the basic principle of the pole-tracking method that will be developed in this work. It is essentially an iteration-based closed-loop parameter-tuning method, where the objective is to ensure the system tracks the reference poles under varying grid SCR. Specifically, the "MSE evaluation" together with the "controller parameter search algorithm" block is in charge of eliminating the tracking error, while the "parameter-pole mapping" is used to predict the poles online using the searched parameters and the newly acquired operating parameters (e.g., k_{SCR}). More details about this diagram are shown in Fig. 2 (b), which will be introduced next.

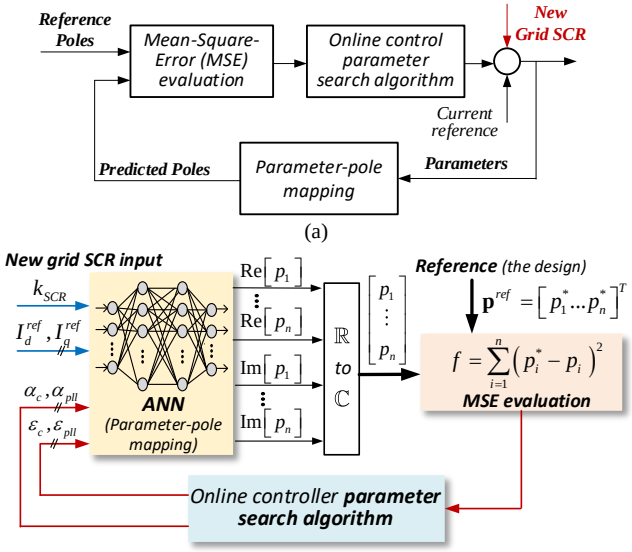

Fig. 2 Schematic of the proposed pole-tracking method. (a) Control diagram illustration of the method. (b) Details about the blocks in (a).

B. Method of the ANN-based parameter-pole mapping

The parameter-pole mapping in Fig. 2 (b) is realized by an ANN. It can be seen that the inputs of the ANN consist of the operating parameters (e.g.,$\boldsymbol{u}_{op}$) and the control parameters (e.g., $\boldsymbol{u}_{ctrl}$, their relations with PI gains of H_{pll}(s) and H_{c}(s) are given in (A.1) of Appendix. B), and defined as:

$$\mathbf{u}_{op}=\left[k_{SCR},I_{cd}^{ref},I_{cq}^{ref}\right] \text{ and } \mathbf{u}_{ctrl}=[\alpha_c,\alpha_{pll},\varepsilon_c,\varepsilon_{pll}] \quad (1)$$

The outputs of the ANN are the real and imaginary parts of the closed-loop system's poles (e.g., $\mathbf{p}=\left[p_1,...,p_n\right]^T$). In this work, they are found by the impedance-based method, where the grid-VSC system in Fig. 1 is represented as a closed-loop control system using the AC admittance (i.e., $\mathbf{Y}_{VSC}$) of the VSC and the grid impedance (i.e., $\mathbf{Z}_{Grid}$) [24][25]. Based on this, the closed-loop poles can be readily calculated from the below equation:

$$\det\left\{\mathbf{I}+\mathbf{Z}_{Grid}(s)\mathbf{Y}_{VSC}(s)\right\}=\mathbf{0} \quad (2)$$

where details of $\mathbf{Y}_{VSC}$ and $\mathbf{Z}_{Grid}$ are given in the Appendix. C. Then, by properly training the ANN using the above-established dataset, the parameter-pole mapping can be obtained, which will be discussed in Section III.A.

C. Method of the parameter search algorithm

As aforementioned, the objective of the parameter-tuning loop is to find a set of $\boldsymbol{u}_{ctrl}$ that ensures the poles under a new grid condition remain close to the reference, i.e., the MSE as depicted in Fig. 2 (b) keeps low. A straightforward but brutal method to fulfill this is to first generate a *high-resolution* parameter space, and second evaluate the distribution of the poles' MSE over the generated space using the ANN (i.e. the parameter-pole mapping); afterwards, control parameters $\boldsymbol{u}_{ctrl}^{new}$

corresponding to the lowest MSE can be directly pinpointed. A two-dimensional case (i.e., assumes two parameters are under tuning) for illustrating this method is shown in Fig. 3 (a). It can be seen that the parameter set (i.e., point *A*) with the lowest MSE can be readily found from the generated parameter space. However, clearly, the precision of this search method relies on the resolution of the generated parameter space. If all of the 4 parameters in $\boldsymbol{u}_{ctrl}$ are to be tuned, the search space will become a *hyperplane*, and the generated data volume for scanning the hyperplane of parameters can be formulated as:

$$N_{vol} = 4 \times \left(N_{spl} \right)^4 \tag{3}$$

where N_{spl} denotes each parameter's search range, i.e., the resolution of this paper. Since a large N_{spl} is expected to be used for this method, the generated data volume will be huge, which is not favorable for online implementations.

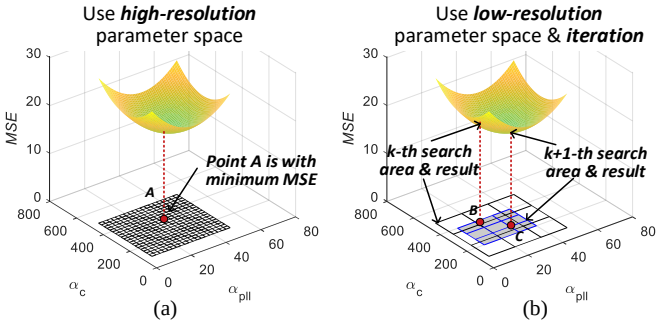

Fig. 3 A two-dimensional example of parameter search methods. Plots are only for illustration purposes. In (b), $N_{spl} = 4$ is demonstrated.

To overcome the above issue, the search of parameters can be decomposed into multiple steps (i.e., using iterations) so that the data resolution for each step can be kept low. As depicted in Fig. 3 (b), a low-resolution parameter space is generated at *k*-step, where the point *B* with the lowest MSE of this step can be found; by using the value of point *B*, the search range of each parameter for the next step are updated, which results in a smaller search area and a new point *C* can be found. This process will be repeated until the MSE corresponding to the searched parameters $\boldsymbol{u}_{ctrl}^{k}$ is satisfactorily low. An algorithm summarizing this iteration-based parameter search method is drawn in Fig. 4, and the main steps are explained below:

Step1: Generate a N_{spl}-samples *vector* for each parameter in $\mathbf{u}_{ctrl}$ at *k*-step using a pre-defined search range, i.e., $\mathbf{u}_{ctrl}^{vt,k} \in \left[\mathbf{u}_{ctrl}^{k,L}, \mathbf{u}_{ctrl}^{k,U} \right]$, where *L*, *U* denote the lower and upper limits for each parameter. Then, a parameter space (e.g., $\mathbf{u}_{ctrl}^{ps,k}$) is spanned by using $\mathbf{u}_{ctrl}^{vt,k}$. It can be obtained that in this work, the dimension of $\mathbf{u}_{ctrl}^{vt,k}$ is $4 \times N_{spl}$, while that of $\mathbf{u}_{ctrl}^{ps,k}$ is $4 \times \left(N_{spl} \right)^4$.

Step 2: Apply $\mathbf{u}_{ctrl}^{ps,k}$ as the inputs to the ANN, the pole space $\mathbf{p}^{ps,k} = \left[\mathbf{p}^k(1), ..., \mathbf{p}^k\left(N_{spl}^4 \right) \right]$ can be numerically obtained, where $\mathbf{p}^k = \left[p_1^k, ..., p_n^k \right]^T$. Based on the pole space, the distribution of MSE is established, from which the index with the lowest MSE (i.e., $n_{f\,\min}^k$) can be identified. Then, corresponding control parameters are extracted from $\mathbf{u}_{ctrl}^{ps,k}$ as: $\mathbf{u}_{ctrl}^{opt,k} = \mathbf{u}_{ctrl}^{ps,k}\left(n_{f\,\min}^k \right)$.

Step 3: Update the upper and lower parameter boundaries for the (*k*+1)-step by using a bisection-like concept as:

$$\mathbf{u}_{ctrl}^{k+1,L/U} = \left(\mathbf{u}_{ctrl}^{opt,k} + \mathbf{u}_{ctrl}^{k,L/U} \right) / 2 \tag{4}$$

The iteration procedure will continue until the condition $MSE < \eta$ is met, where η is a predefined tolerance. Notably, termination of the iteration also indicates that the VSC will achieve the *pole-tracking* when $\mathbf{u}_{ctrl}^{opt,k}$ is applied.

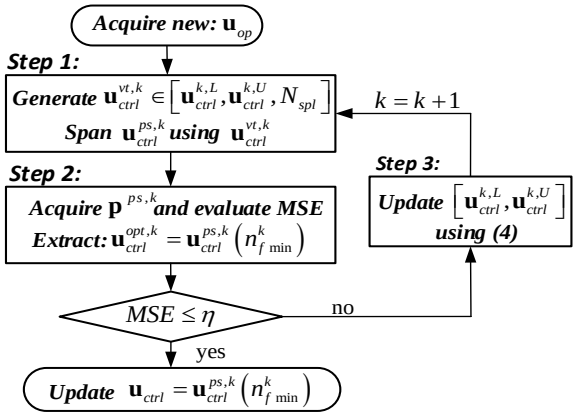

Fig. 4 Flowchart of the parameter search algorithm for pole-tracking.

III. Implementation and Simulation Results

A. Implementation of the pole-tracking method

1) Implementation of the parameter-pole mapping

As mentioned earlier, the dataset for ANN training consists of $\boldsymbol{u}_{op}, \boldsymbol{u}_{ctrl}$ and corresponding poles. In this work, it is achieved by modeling $\mathbf{Z}_{Grid}(s)$, $\mathbf{Y}_{VSC}(s)$ as symbolic functions of $\boldsymbol{u}_{op}, \boldsymbol{u}_{ctrl}$ in MATLAB; then calculating the poles according to (2), which are functions of $\boldsymbol{u}_{op}, \boldsymbol{u}_{ctrl}$ as well; finally, by sweeping $\boldsymbol{u}_{op}, \boldsymbol{u}_{ctrl}$ over the below-defined parameter ranges, the numeric poles for ANN training are obtained:

$$\begin{aligned} \left[\mathbf{u}_{ctrl}^{L}, \mathbf{u}_{op}^{L} \right] &= \left[100 \quad 5 \quad 0.2 \quad 0.2 \quad 2 \quad -20A \quad -20A \right] \\ \left[\mathbf{u}_{ctrl}^{U}, \mathbf{u}_{op}^{U} \right] &= \left[500 \quad 50 \quad 1.2 \quad 1.2 \quad 12 \quad +20A \quad +20A \right] \end{aligned} \tag{5}$$

It is worth mentioning that to acquire various combinations of input parameters to a greater extent and with a relatively low data volume, the samples of each parameter in $\boldsymbol{u}_{op}, \boldsymbol{u}_{ctrl}$ are generated by random numbers subject to the uniform distribution and within the above ranges, i.e.,

$$\mathbf{u}_{in} = \begin{bmatrix} \mathbf{u}_{op}(1), ..., \mathbf{u}_{op}(k), ..., \mathbf{u}_{op}(N) \\ \mathbf{u}_{ctrl}(1), ..., \mathbf{u}_{ctrl}(k), ..., \mathbf{u}_{ctrl}(N) \end{bmatrix} \tag{6}$$

where $\mathbf{u}_{op}(k)$ and $\mathbf{u}_{op}(k)$ subject to (3) and the uniform distribution. Accordingly, the pole samples can be obtained as:

$$\mathbf{y}_{poles} = \begin{bmatrix} \mathbf{p}_1(1) & \cdots & \mathbf{p}_1(N) \\ \mathbf{p}_2(1) & \cdots & \mathbf{p}_2(N) \\ \vdots & & \vdots \\ \mathbf{p}_n(1) & \cdots & \mathbf{p}_n(N) \end{bmatrix} \tag{7}$$

where $\mathbf{y}_{poles}(k)$ denotes the system's poles evaluated at $\mathbf{u}_{in}(k)$.

In this study, the number of samples in (6) and (7) is $N = 400$, thus $\mathbf{u}_{in}$ is a 7×400 dimensional matrix. Since the system has 6 complex poles (this will be shown in a later offline test of the pole-tracking method), $\mathbf{y}_{poles}$ is a 6×400 dimensional matrix. It should be noted that for ANN training, the dataset should be formulated as real numbers, thus the poles are further separated into real and imaginary parts, and the resulting output samples will be a 12×400 dimensional matrix as:

$$\mathbf{y}_{out} = \left[\mathrm{Re}\left\{\mathbf{y}_{poles}\right\}; \mathrm{Im}\left\{\mathbf{y}_{poles}\right\} \right] \tag{8}$$

Based on the dataset (6) and (8), the ANN can be trained in the environment of MATLAB. A trained result along with the applied configurations is shown in Fig. 5. This ANN will serve as the parameter-pole mapping of this work.

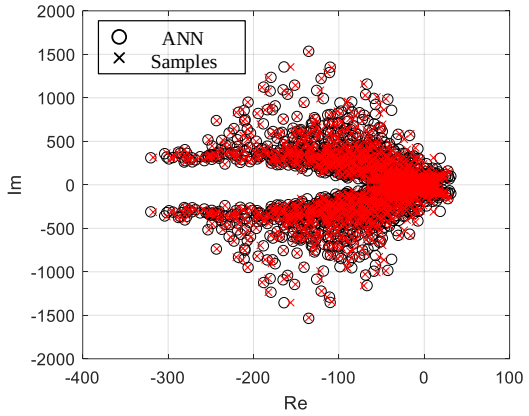

Fig. 5. The trained ANN. A forward neural network with 3 hidden layers and having [7, 8, 6] hidden neurons in each layer is used. The active functions for each layer are {'tansig', 'logsig', 'logsig'} and the standard backpropagation learning algorithm is deployed for training. Besides, 30% of the dataset is used for validation.

2) Implementation of the parameter search algorithm

The parameter search algorithm of Fig. 4 can be readily implemented with MATLAB script based on the elaborations in Section II.C. In which, the parameter vector $\mathbf{u}_{ctrl}^{vt,k}$ is generated by the command *linspace()* with a resolution $N_{spl} = 3$; using the generated parameter vectors, the parameter space $\mathbf{u}_{ctrl}^{ps,k}$ can be further spanned by the command *ndgrid()*.

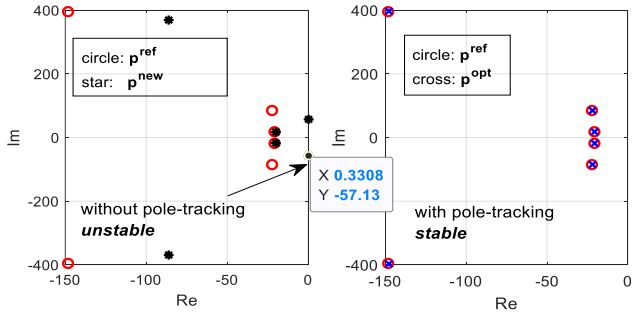

Fig. 6 Offline test of the effect of the pole-tracking method.

An offline test of this algorithm is shown in Fig. 6. In which, the reference poles (i.e., $\mathbf{p}^{ref}$) of this case are set using the conditions: $\mathbf{u}_{op}^{ref} = [\mathbf{10}, 10A, 0A]$, $\mathbf{u}_{ctrl}^{ref} = [200, 20, 0.707, 0.707]$ and the results are shown in Fig. 6 (left-side). Then a new condition $\mathbf{u}_{op}^{new} = [\mathbf{4}, 10A, 0A]$ is assigned to emulate the change of grid SCR (i.e., from 10 to 4); under this new condition, two sets of poles will be obtained: one set of poles (i.e., $\mathbf{p}^{new}$) is obtained with the pole-tracking disabled (i.e., the $\mathbf{u}_{ctrl}^{new} = \mathbf{u}_{ctrl}^{ref}$), while the other set of poles (i.e., $\mathbf{p}^{opt}$) is obtained with the pole-tracking enabled (i.e., $\mathbf{u}_{ctrl}^{opt} \neq \mathbf{u}_{ctrl}^{ref}$). By comparing the plots of $\mathbf{p}^{ref}, \mathbf{p}^{new}, \mathbf{p}^{opt}$, it can be clearly seen that without pole-tracking the system will be unstable under the new grid condition (see the marked data in Fig. 6 (where a pair of unstable poles is presented); while stability can be retained when the pole-tracking feature is enabled (the poles are pulled back to the reference as can be seen from the right-side figure).

It is worth mentioning that for online implementation of this method, the iteration-based parameter search algorithm is separated and fulfilled by multiple control cycles. This means, for each control cycle, only one iteration is allocated and proceeded. In this manner, the computational effort required by each control cycle can be made low.

Table I Main system configurations

Configuration for simulation and experimental setup			
Name	Value	Name	Value
U_N (rms)	230 V	L_f	4.4 mH
S_N (3-phase)	10 kVA	L_g	L_{base}/k_{SCR}
V_{dcN}	750V	L_{base}	0.052 H
f_{SW}	10 kHz	T_{ctrl}	100 μs
Configuration for the parameter search algorithm			
N_{spl}	3	η	10^{-3}
dim of $\boldsymbol{u}_{ctrl}^{vt,k}$	4×3	dim of $\boldsymbol{u}_{ctrl}^{ps,k}$	4×81
dim of $\boldsymbol{p}^{k}$	6×1	dim of $\boldsymbol{p}^{ps,k}$	6×81
Note: "dim" denotes the dimension; an averaged MSE with five samples is compared with η for online application.			

B. Online simulation test of the pole-tracking method

Simulation in MATLAB is conducted to test the online version of the algorithm. At 0.5s, an additional grid inductor is inserted into the circuit, which will result in a new grid SCR as $k_{SCR}^{new} = 4$ (i.e., a relatively weak grid). Initial control parameters are the same as $\mathbf{u}_{ctrl}^{ref}$ used in Fig. 6, other circuit parameters are given in Table I.

From the current waveforms in Fig. 7 (a), it can be clearly seen that without the pole-tracking feature the system becomes unstable when the new grid SCR presents, while the system can be stabilized when it is enabled, these simulation results are consistent with those in Fig. 6.

On the other side, the waveform of MSE in Fig. 7 (b) further depicts how the search algorithm works, where the MSE is reduced step by step, while the overall time required to find the new parameters is approximately 4 *ms* in the presented case, which is well below one system period. Although the presented performance of the pole-tracking method is considered to be sufficient, it is noteworthy to mention that additional savings of computation-time can be achieved by compromising the accuracy of pole-tracking.

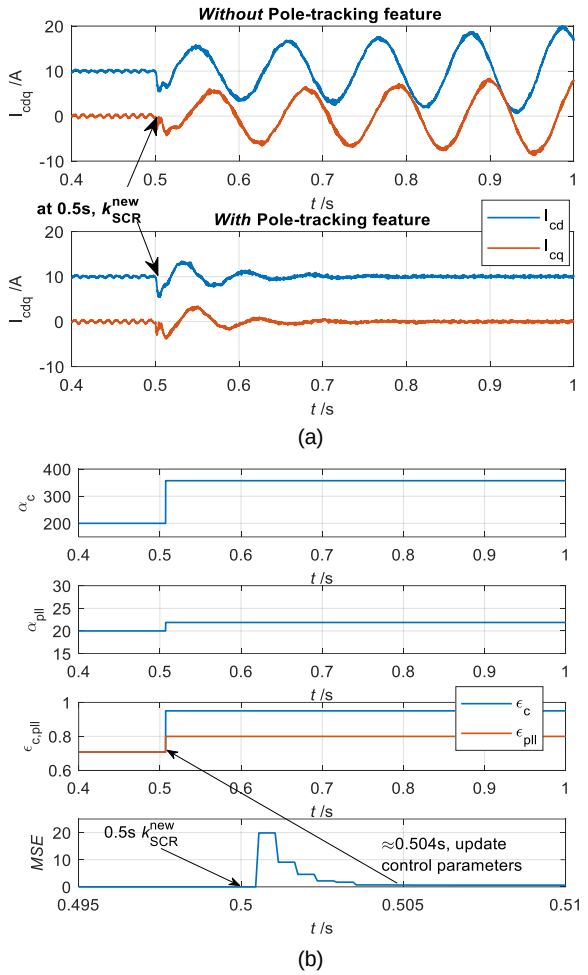

Fig. 7 Simulation test of the proposed pole-tracking method (a) Comparison of current waveforms; (b) Waveforms of control parameter update in response to the change of k_{SCR}.

IV. Experimental Validation

The experimental setup is shown in Fig. 8. The control system along with the developed method is digitally implemented in dSPACE with a control cycle T_{ctrl} = 100 μs. The VSC comprises IGBT stack (Danfoss VLT302) switching at f_{SW} = 10 kHz. In the experiment, the change of k_{SCR} from 11.3 to 4 is achieved by inserting an additional inductance (i.e., L_{g2} in the figure) into the main circuit. The reference poles are set using: $\mathbf{u}_{op\_exp}^{ref} = [\mathbf{11.3}, 10A, 5A]$ and $\mathbf{u}_{ctrl\_exp}^{ref} = [130, 15, 0.7, 0.65]$; while a new operating condition as: $\mathbf{u}_{op\_exp}^{new} = [\mathbf{4}, 10A, 5A]$ will be obtained when L_{g2} is inserted in the circuit. It can be readily tested offline with the ANN (similar to the analysis of Fig. 6) that under this new condition (i.e., $\mathbf{u}_{op\_exp}^{new}$), the system is anticipated to be *unstable* with the original control parameters (i.e., $\mathbf{u}_{ctrl\_exp}^{ref}$), thus parameter-tuning is desired in this case. Experimental validation of the pole-tracking method under this scenario is conducted and the main results are discussed below.

As shown in Fig. 9, the pole-tracking method is triggered back and forth three times (see 1st, 2nd, 3rd) by interchangeably using the operating conditions $\mathbf{u}_{op\_exp}^{new}$ and $\mathbf{u}_{op\_exp}^{ref}$ to test the consistency of the algorithm. It can be seen that when L_{g2} is inserted in the circuit, the VSC's currents tend to oscillate indicating instability, this consists with the above analysis that under the new grid SCR (i.e., $\mathbf{u}_{op\_exp}^{new}$), the initial control parameters (i.e., $\mathbf{u}_{ctrl\_exp}^{new}$) cannot ensure the stability of the system. When the pole-tracking is enabled (see the mark "1st" in the subplot of "flag") with the new condition $\mathbf{u}_{op\_exp}^{new}$ for online parameter tuning, it can be observed that the system regains its stability immediately by updating the searched control parameters (see the waveforms of $\alpha_{c,pll}, \varepsilon_{c,pll}$). Moreover, the stepwise decrease of MSE indicates the pole-tracking is gradually achieved as expected.

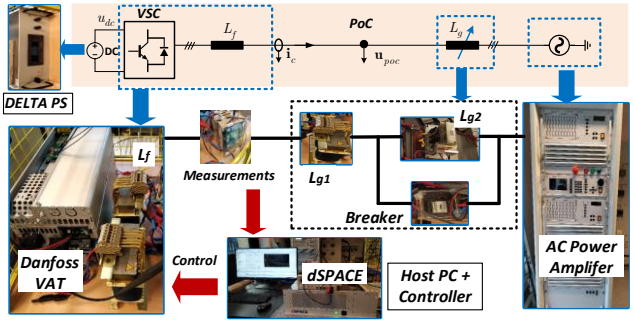

Fig. 8 Experimental setup. In which, Lg1 = 4.4 mH, Lg2 = 8.2 mH. Other circuit parameters are the same as Table I

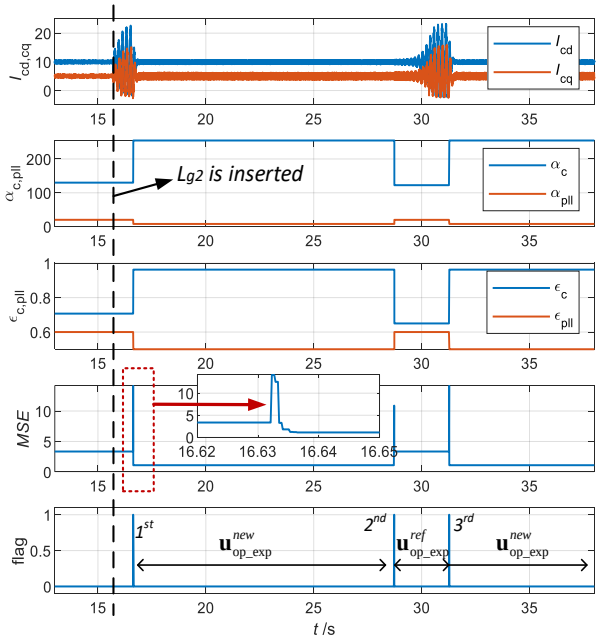

Fig. 9 Experimental testing waveforms of the pole-tracking method.

On the other hand, from the plots regarding the 2nd triggering instance it can be seen that although the initial control parameters (i.e., $\mathbf{u}_{ctrl\_exp}^{ref}$) can be successfully found, the system shows instability again. This is not surprised as the VSC is currently operating under a weak grid (i.e., $k_{SCR}^{new} = 4$) while the parameter tuning is fed with the wrong grid information (i.e., $k_{SCR}^{ref} = 11.3$ in $\mathbf{u}_{op\_exp}^{ref}$). By contrast, when the 3rd triggering instance comes (where the correct grid information is used), the system regains its stability and the searched control parameters are the same as those of the 1st triggering instance. This analysis demonstrates the consistency of the algorithm.

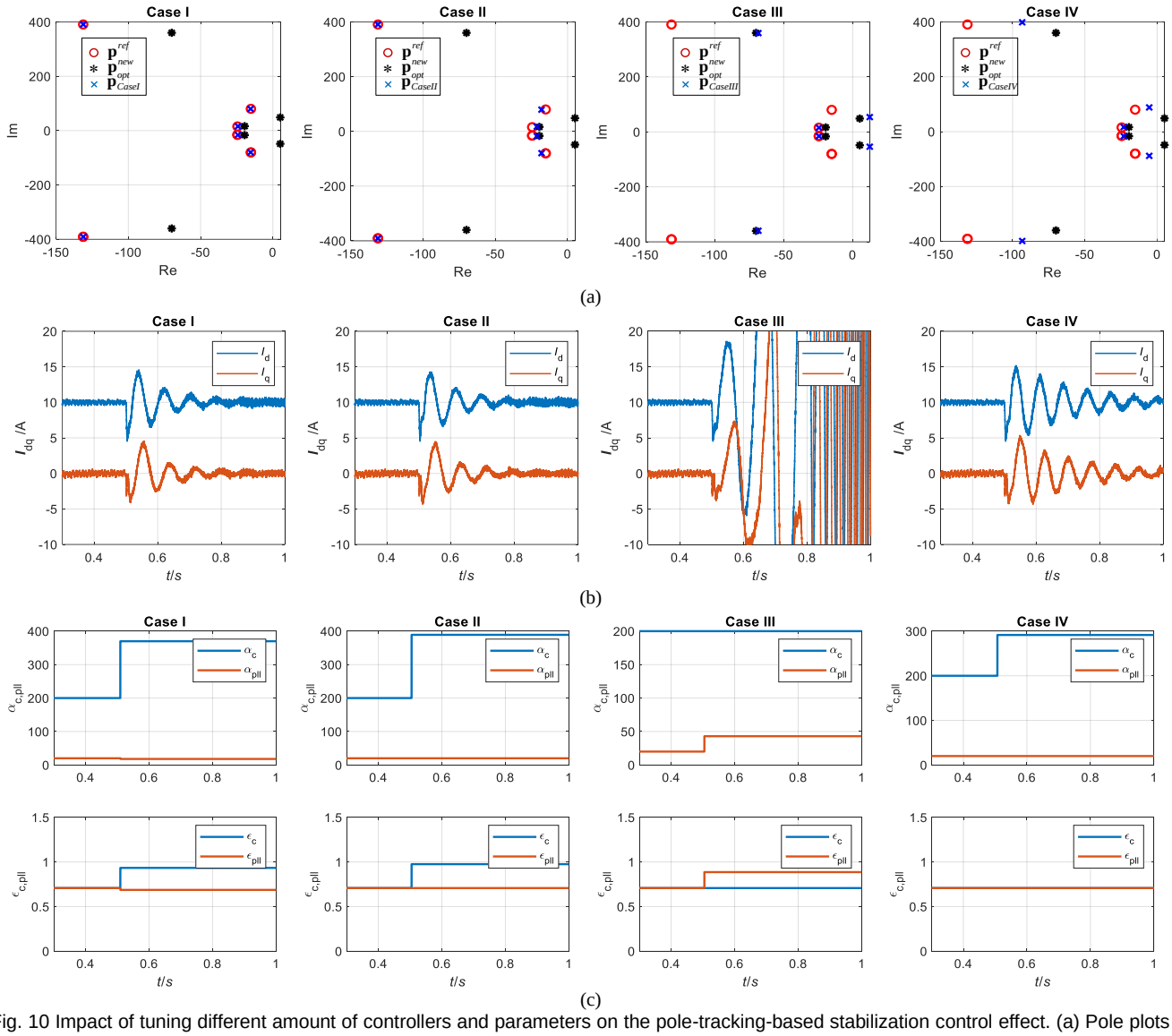

Fig. 10 Impact of tuning different amount of controllers and parameters on the pole-tracking-based stabilization control effect. (a) Pole plots of Case I~IV. (b) Time-domain waveforms of Case I~IV. (c). Control parameter update corresponding to time-domain waveforms of Case I~IV.

Overall, this experiment further consolidates the efficacy of the pole-tracking method in online stabilization control of the VSC, particularly its applicability in real-time control systems is demonstrated.

V. Discussion

The above analysis also shows that the successful realization of the pole-tracking method can be greatly credited to the low computation effort of the ANN-based parameter-pole mapping and the multi-parameter tuning ability of the search algorithm. In particular, the latter ability is crucial for tuning MIMO systems as earlier mentioned. To further show this effect, tuning the different amount of controllers and parameters on the impact of the pole-tracking performance will be discussed in this section, for which the following cases are arranged:

Case I: All the four control parameters in $\boldsymbol{u}_{\text{ctrl}}$ are tuned;
Case II: Only α_c *and* ϵ_c of the current controller are tuned;
Case III: Only α_{pll} *and* ϵ_{pll} of the PLL are tuned;
Case IV: Only α_c is tuned.

The main results of this study are given in Fig. 10. First, Fig. 10 (a) shows the pole plots of Case I~IV, where the '*red circle*' denotes the reference poles $\mathbf{p}^{ref}$ obtained using the conditions: $\mathbf{u}_{ctrl}^{ref}=[200,20,0.707,0.707]$ and $\mathbf{u}_{op}^{ref}=[\mathbf{8},10A,0A]$ (see Appendix. B for more explanations); *'black star'* denotes the system's new poles (i.e., $\mathbf{p}^{new}$) under the new grid SCR (i.e., $k_{SCR}^{new}=3$ is applied); while the *'blue cross'* denotes the poles (i.e., $\mathbf{p}_{CaseI}^{opt}$, $\mathbf{p}_{CaseII}^{opt}$, $\mathbf{p}_{CaseIII}^{opt}$, $\mathbf{p}_{CaseIV}^{opt}$) resulting from the parameter tuning. By observing Fig. 10 (a), the following results can be directly obtained:

1) From the pole-plot of Case I it can be seen that the system under the new grid SCR will be unstable due to the presence of a pair of unstable poles in $\mathbf{p}^{new}$; while an excellent pole-tracking performance is anticipated by tuning the parameters of the current controller and the PLL simultaneously.

2) By comparing Case II and III, it can be clearly obtained that tuning the current controller is more effective than solely tuning the PLL because Case II is stable while Case III is not.

3) When comparing Case I and II more in detail, it can be seen that the pole-tracking performance with solely tuning the current controller is not as good as that of tuning all of them. This is because the system's poles are functions of all the control parameters (i.e., a MIMO system), thus only tuning of a few of them may not reach a satisfactory result, e.g., in Case III, merely tuning PLL cannot ensure the stability of this study.

4) The plot of Case IV shows that although solely tuning α_c can ensure the stability of this study, the effect of the stabilization control is anticipated to be weaker compared with Case I and II. This is because the dominant poles (poles closest to the imaginary axis) of Case IV are more close to the imaginary axis, which implies less damping of the system.

The above offline pole-tracking analysis can be readily certified by the presented online testing waveforms in Fig. 10 (b) and (c). In which Case III is unstable as predicted, Case III though is stable the response is poorer than Case I and II due to less damping. This comparative analysis in general better demonstrates the significance of multi-parameter tuning ability in MIMO systems' applications.

VI. Conclusion

This paper presented a pole-tracking-based parameter tuning method aiming for online stabilization control of the grid-tied VSC. The method endows the VSC with a novel pole-tracking feature by which stability of the VSC under changing grid conditions can be ensured. Experimental results demonstrated the efficacy of the proposed method in real-time applications.

The enabling technique behind the pole-tracking method is the developed online parameter search algorithm that can effectively and simultaneously tune multi controllers and parameters. This ability is particularly desired for tuning MIMO systems with evident couplings. In addition, the proposed method is user friendly, only a set of reference poles need to be specified (in this work, it is set simply by using a strong grid condition, see Appendix. B), while the tuning law for pole-tracking is automatically achieved by the iteration-based parameter tuning loop, i.e., the parameter search algorithm.

Despite this, it is worth remarking that the reference poles is in fact another degree of control freedom that can be utilized, e.g., they can be more specifically designed to achieve a certain optimal performance or to ensure the tracking ability over a wider range of grid parameter variations. Besides, in cases that tuning all of the control parameters is not readily attainable (e.g., a high-order and complex system), selective tracking (e.g., prioritize the tracking of dominant poles) can be the relevant technique to be considered. In future work, these interesting topics will be explored to further enrich the features of the presented pole-tracking method.

Appendix

A. Nomenclature and abbreviations

"sim":	simulation;	"ref":	reference;
"exp":	experiment;	"*N*":	nominal;
"ps":	parameter space;	"vt":	vector;
"ctrl":	control	"op":	operating
"opt":	optimized	"SW":	switching
"c":	converter	"pll":	phase-locked-loop
"g":	grid	"f":	filter
"spl":	sample	"vol":	volume
"L":	lower	"U":	upper

Symbols using the above abbreviations or their combinations as the sub or superscripts denote the variables or constants related to the implications of those abbreviations.

B. Design of the PI controller gains and the setting of the reference poles

In this work, the reference poles are set by a set of control parameters designed under a strong grid condition. When the grid is assumed strong, the current control loop (CCL) and PLL are nearly decoupled thus can be designed individually (i.e., an open-loop design approach). Since both CCL and PLL of this study are second-order systems (in a small signal sense), if the below PI gains of the current controller and PLL are applied:

$$\begin{aligned} &H_c(s): k_{pc} = 2\alpha_c L_f, k_{ic} = \left(\alpha_c / \varepsilon_c\right)^2 L_f \\ &H_{pll}(s): k_{ppll} = 2\alpha_{pll} / U_N, k_{ipll} = \left(\alpha_{pll} / \varepsilon_{pll}\right)^2 / U_N \end{aligned} \tag{A.1}$$

In this manner, α_c and α_{pll} will approximately characterize how fast the time-domain responses of CCL and PLL will settle (as they are reciprocal to the time constants of corresponding second-order systems), while ε_c and ε_{pll} mainly affects the resonance frequencies. Once the PI gains are obtained from the above open-loop design, the reference poles can be set by using a strong grid condition (i.e., use a relatively large k_{SCR} in $\mathbf{u}_{op}^{ref}$).

C. dq-domain impedance models of VSC and grid

$\mathbf{Z}_{VSC} = \left(\mathbf{I} + \mathbf{G}_{pllu}\right)^{-1}\left(sL_f + H_c\right)$, $\mathbf{Z}_{Grid} = \begin{bmatrix} sL_g & -\omega_1 L_g \\ \omega_1 L_g & sL_g \end{bmatrix}$ where $\mathbf{G}_{pllu} = \begin{bmatrix} I_{cq}H_c \\ -\left(I_{cd}H_c + U_{poc}\right) \end{bmatrix}[0 \quad G_{pll}]$, $G_{pll} = \dfrac{H_{pll}}{s + U_{poc}H_{pll}}$. One may refer to [25] for detailed *dq*-impedance modeling method.

Acknowledgment

The authors would like to thank Mr. Pere Izquierdo Gómez for valuable discussions on AI techniques, and PowerLabDK of DTU for offering lab facilities during the course of the work.

References

[1] J. Khazaei, P. Idowu, A. Asrari, A. Shafaye, L. Piyasinghe. "Review of HVDC control in weak AC grids," in *Electric power systems research*, vol. 162, pp. 194-206, Sep. 2018.

[2] IEEE Guide for Planning DC Links Terminating at AC Locations Having Low Short-Circuit Capacities, IEEE Standard 1204-1997, 1997.

[3] H. Liu, X. Xie, J. He, J, T. Xu, Z. Yu, C. Wang, C. Zhang, "Subsynchronous Interaction Between Direct-Drive PMSG Based Wind Farms and Weak AC Networks," in IEEE Transactions on Power Systems, vol. 32, no. 6, pp. 4708-4720, Nov. 2017.

[4] C. Li, "Unstable Operation of Photovoltaic Inverter from Field Experiences," in *IEEE Transactions on Power Delivery*, Vol. 33, No. 2, April 2018, pp. 1013-1015.

[5] J. Sun, "Impedance-Based Stability Criterion for Grid-Connected Inverters," in IEEE Transactions on Power Electronics, vol. 26, no. 11, pp. 3075-3078, Nov. 2011, doi: 10.1109/TPEL.2011.2136439.

[6] R. D. Middlebrook, "Input filter considerations in design and applications of switching regulators," in Proc. IEEE Ind. Appl. Soc. Annu. Meeting, 1976, pp. 91-107.

[7] M. Belkhayat, “Stability criteria for AC power systems with regulated loads,” Ph.D. dissertation, Purdue University, USA, 1997.
[8] H. A. Young, M. A. Perez and J. Rodriguez, "Analysis of Finite-Control-Set Model Predictive Current Control With Model Parameter Mismatch in a Three-Phase Inverter," in IEEE Transactions on Industrial Electronics, vol. 63, no. 5, pp. 3100-3107, May 2016.
[9] R. P. Vieira, L. T. Martins, J. R. Massing and M. Stefanello, "Sliding Mode Controller in a Multiloop Framework for a Grid-Connected VSI With LCL Filter," in IEEE Transactions on Industrial Electronics, vol. 65, no. 6, pp. 4714-4723, June 2018.
[10] N. Hoffmann and F. W. Fuchs, "Minimal Invasive Equivalent Grid Impedance Estimation in Inductive–Resistive Power Networks Using Extended Kalman Filter," in IEEE Transactions on Power Electronics, vol. 29, no. 2, pp. 631-641, Feb. 2014.
[11] I. Jarraya, J. Hmad, H. Trabelsi, A. Houari and M. Machmoum, "An Online Grid Impedance Estimation Using Recursive Least Square For Islanding Detection," 2019 16th International Multi-Conference on Systems, Signals & Devices (SSD), 2019, pp. 193-200.
[12] P. García, M. Sumner, Á. Navarro-Rodríguez, J. M. Guerrero and J. García, "Observer-Based Pulsed Signal Injection for Grid Impedance Estimation in Three-Phase Systems," in IEEE Transactions on Industrial Electronics, vol. 65, no. 10, pp. 7888-7899, Oct. 2018.
[13] T. Roinila, M. Vilkko and J. Sun, "Broadband methods for online grid impedance measurement," 2013 IEEE Energy Conversion Congress and Exposition, 2013, pp. 3003-3010, doi: 10.1109/ECCE.2013.6647093.
[14] K. J. Åström, T. Hagglund. Revisiting the Ziegler-Nichols step response for PID control. Journal of Process Control, 2004, 14:635~650.
[15] S. Moon, L. Corradini and D. Maksimović, "Autotuning of Digitally Controlled Boost Power Factor Correction Rectifiers," in IEEE Transactions on Power Electronics, vol. 26, no. 10, pp. 3006-3018, Oct. 2011, doi: 10.1109/TPEL.2011.2125802.
[16] Q. Liu, T. Caldognetto and S. Buso, "Stability Analysis and Auto-Tuning of Interlinking Converters Connected to Weak Grids," in IEEE Transactions on Power Electronics, vol. 34, no. 10, pp. 9435-9446, Oct. 2019, doi: 10.1109/TPEL.2019.2899191.
[17] A. Khodamoradi, G. Liu and P. Mattavelli, "Online Controller Tuning for DC Microgrid Power Converters With the Ability to Track Maximum Allowable Bandwidth," in IEEE Transactions on Industrial Electronics, vol. 69, no. 2, pp. 1888-1897, Feb. 2022, doi: 10.1109/TIE.2021.3057009.
[18] A. Rygg, M. Molinas, C. Zhang and X. Cai, "A Modified Sequence-Domain Impedance Definition and Its Equivalence to the dq-Domain Impedance Definition for the Stability Analysis of AC Power Electronic Systems," in IEEE Journal of Emerging and Selected Topics in Power Electronics, vol. 4, no. 4, pp. 1383-1396, Dec. 2016.
[19] S. Li, M. Fairbank, C. Johnson, D. C. Wunsch, E. Alonso and J. L. Proao, "Artificial Neural Networks for Control of a Grid-Connected Rectifier/Inverter Under Disturbance, Dynamic and Power Converter Switching Conditions," in IEEE Transactions on Neural Networks and Learning Systems, vol. 25, no. 4, pp. 738-750, April 2014.
[20] M. Zhang, X. Wang, D. Yang and M. G. Christensen, "Artificial Neural Network Based Identification of Multi-Operating-Point Impedance Model," in IEEE Transactions on Power Electronics, vol. 36, no. 2, pp. 1231-1235, Feb. 2021.
[21] M. Novak and T. Dragicevic, "Supervised Imitation Learning of Finite-Set Model Predictive Control Systems for Power Electronics," in *IEEE Transactions on Industrial Electronics*, vol. 68, no. 2, pp. 1717-1723, Feb. 2021.
[22] M. Hajihosseini, M. Andalibi, M. Gheisarnejad, H. Farsizadeh and M. Khooban, "DC/DC Power Converter Control-Based Deep Machine Learning Techniques: Real-Time Implementation," in *IEEE Transactions on Power Electronics*, vol. 35, no. 10, pp. 9971-9977, Oct. 2020.
[23] S. Zhao, F. Blaabjerg and H. Wang, "An Overview of Artificial Intelligence Applications for Power Electronics," in IEEE Transactions on Power Electronics, vol. 36, no. 4, pp. 4633-4658, April 2021.
[24] C. Zhang, M. Molinas, A. Rygg and X. Cai, "Impedance-Based Analysis of Interconnected Power Electronics Systems: Impedance Network Modeling and Comparative Studies of Stability Criteria," in IEEE Journal of Emerging and Selected Topics in Power Electronics, vol. 8, no. 3, pp. 2520-2533, Sept. 2020.
[25] B. Wen, D. Boroyevich, R. Burgos, P. Mattavelli and Z. Shen, "Small-Signal Stability Analysis of Three-Phase AC Systems in the Presence of Constant Power Loads Based on Measured d-q Frame Impedances," in IEEE Transactions on Power Electronics, Vol. 30, No. 10, October 2015, pp. 5952-5963.